Scattering of low-energy positrons by helium and neon atoms

P. G. Coleman, J. D. McNutt, L. M. Diana, and J. R. Burciaga*
Department of Physics, The University of Texas at Arlington, Arlington, Texas 76019
(Received 31 July 1978)

Total cross sections for the scattering of 2–50 eV positrons by helium and neon atoms have been measured using the time-of-flight technique, and are compared with recent experimental and theoretical results. The measurement of positron energies and the flight path length is described and possible sources of systematic errors, including the effects of small-angle forward scattering, are fully discussed.

I. INTRODUCTION

The reemission of a small fraction of incident fast positrons from a solid target with a spectrum of low energies peaked at about 1 eV is a process which has been exploited in a variety of experimental investigations during the past decade. Among these are measurements of total scattering cross sections,[1-5] studies of the formation of positronium in both the ground and first excited states,[6,7] and the investigation of surface properties of solids.[8]

Although there have been theoretical[9] and experimental[10] studies of the positron energy moderation process, a complete understanding of the mechanism is yet to be gained. Theoretical research in this area has focused on the model wherein the fast positrons entering a solid are thermalized close to its surface and are subsequently ejected under the influence of a negative work function. Experimental verification of this model will require meticulous surface preparation and corrections for systematic effects such as contact potential differences. Stein *et al.*[11] reported the emission of positrons of mean energy $\bar{E} < 1$ eV and with a near-thermal energy width from a boron sample coated with cracked pump oil. In contrast, the energy spectra of slow positrons emitted from MgO are characterized by $\bar{E} \approx 1.6$ eV and width ≈ 1 eV; it is shown below that this larger energy spread can sometimes be profitably exploited.

The total cross-section measurements reported here for positron-helium and positron-neon scattering were prompted by discrepancies which exist among previously measured values,[2,3,5] especially at energies less than 10 eV. The apparatus was therefore specifically designed to facilitate measurements in this energy range. Throughout the experimental program the shape and intensity of the slow-positron spectra were monitored, and systematic effects were examined closely in an attempt to obtain more information on the behavior of MgO as a positron moderator.

The experimental system and the data analysis techniques are described in Secs. II and III, respectively. The results of the studies of positron energy moderation in MgO are presented and discussed in Sec. IV. In Sec. V, the procedure by which total cross sections are obtained from the measured energy spectra is described, and experimental errors are analyzed. Finally, in Sec. VI, the measured total cross sections for positron-helium and positron-neon scattering are reported and compared with previous experimental and theoretical results.

II. TIME-OF-FLIGHT SPECTROMETER

The time-of-flight (TOF) spectrometer used for the measurements is represented schematically in Fig. 1. The basic features of the system developed by Coleman *et al.*[12] are retained. Fast positrons (maximum energy $\simeq 0.54$ MeV) from a ^{22}Na source pass into the evacuated flight tube through a 0.05 mm thick aluminized Mylar window, 2 mm from which is positioned an insulated 325 gauge 40% transmission stainless-steel grid. This grid is coated thinly with MgO powder, which is deposited by burning magnesium ribbon in air approximately 100 mm beneath the grid immediately prior to its installation in the system.

Approximately 1 in 10^5 of the positrons passing through the Mylar window are moderated into a peaked spectrum of low energies through interaction with the MgO powder grains. A similar efficiency was noted when a 92% transmission tungsten grid was used to support the powder, suggesting that the composition and structure of the grid are relatively unimportant in this regard and that the role of the grid in producing the moderated beam is small. It appeared, however, that the stainless-steel-grid–MgO system was less susceptible to the charging effects discussed in Sec. IV. Application of a potential V between the coated

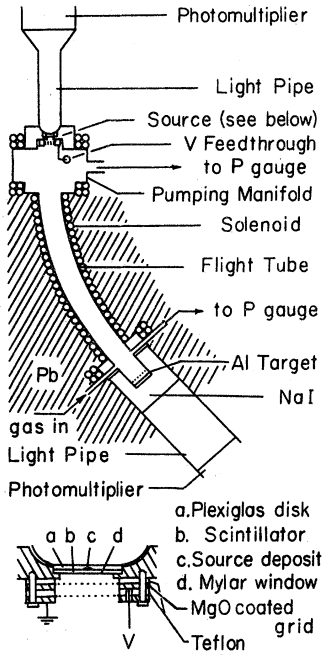

FIG. 1. Schematic diagram of TOF spectrometer, to scale.

grid and a fine tungsten grounded grid 2 mm away, allows acceleration of the forward-going slow positrons to any desired mean energy.

The slow positrons then enter a curved, evacuated brass flight tube of length 0.33 m and diameter 20 mm, and are guided by an axial magnetic field to an aluminum target at the end of the tube upon which they are annihilated. The target disk is insulated from the flight tube by a Teflon gasket and is maintained at −150 V at a distance of 5 mm behind a second grounded tungsten grid. This arrangement insures that the slow positrons are promptly drawn back to the target if they are initially backscattered from it.

Gases are leaked into the system through a micrometering valve situated 25 mm from the target, and are continuously pumped through the flight tube to avoid possible accumulation of impurity atoms in the system. An aluminum gate valve above a 5-cm diffusion pump, which when fully opened allows pumping of the system to a base pressure of 5×10^{-8} Torr, is adjusted to reduce the gas flow so that a pressure gradient of 10% is maintained between the two ends of the flight tube. The flow rate under these conditions is about $6\times10^{-4}P$ 1 s^{-1}, where P is the mean gas pressure in the system in Torr at room temperature.

Pressure measurements are made at two ports 25 mm from each end of the flight tube using a Baratron capacitance manometer (1-Torr head). The values of pressure used in the calculation of total cross sections were measured with both ports simultaneously open to the gauge head. The pressure measured in this manner was consistently found to be equal to the mean of the port pressures measured independently. Corrections to the pressure readings related to changes in gradient in the 25-mm sections between the measuring ports and the tube ends are self-cancelling and are considered to be negligible. In order to calculate atomic number densities, the temperature T of the flight tube was measured with a thermocouple gauge. When a high current of 2.5 A is passed through the solenoid coils $T\approx33$ °C, but the normal operating current of about 0.4 A produces no noticeable heating above room temperature.

Measurement of a positron energy spectrum is achieved by timing individual positrons along the flight tube, using fast electrical timing pulses taken from photomultiplier tubes located at each end of the system. These photomultipliers detect light flashes (a) produced by ^{22}Na positrons as they pass through a 0.25 mm thick disk of KL236 plastic scintillator located directly behind the Mylar window (the time interval between detection of a fast positron and the subsequent emission of a moderated positron is assumed to be negligible) and (b) from a 5-cm NaI(Tl) well crystal, which nearly surrounds the target, as it detects one or both of the annihilation quanta. Both photomultiplier tubes are optically coupled to their scintillators by Plexiglas light pipes which serve to remove them from regions where the residual magnetic fields would adversely affect their performance. To avoid the flooding of the NaI crystal by emission and annihilation gamma rays from the source region, which would contribute to a high background counting rate, the flight tube is curved on an arc of radius 200 mm and is incased in lead.

Pulses from the photomultiplier tubes are fed via constant-fraction discriminators into the start and stop inputs of a time-to-amplitude converter (TAC). Because the source pulse rate is about 5×10^{5} s^{-1} and the target pulse rate is less than 10^{2} s^{-1}, the emission pulses are delayed (using low-loss delay cable) and used as TAC stop pulses, whereas the annihilation pulses are used to start the TAC. In this way, the loss of 95% of the TAC start pulses—those which would arrive at the TAC input while the system is busy—is averted. The TAC output pulses, whose height is proportional to the time interval between receipt of start and stop pulses, pass to a multichannel analyzer (MCA) which sorts and stores them according to their height into 200 channels, and a time-of-flight histogram is collected.

Side-channel energy gating is employed in order to improve the signal-to-background ratio by pre-

ferentially selecting those NaI detector pulses associated with 0.51-MeV annihilation quanta. This is achieved by gating the MCA input with pulses from a single channel analyzer (SCA) which correspond to those amplified dynode pulses from the target photomultiplier whose heights lie between preselected limits. It was found that the SCA window could be extended from just below the small 1.28-MeV photopeak, which results from the detection of gamma photons emitted by the ^{22}Na, to well down into the 0.51-MeV Compton scattering shoulder with no noticeable deterioration in the signal-to-background ratio. A timing resolution of 4.4 ns was maintained.

Energy gating reduces the effective start-pulse rate to about 25 s^{-1}. However, over half of these pulses are prompt-related to pulses in the stop (i.e., the emission) pulse train. These pulses may be prematurely converted by unrelated stop pulses, resulting in background "events" lying beneath the delayed signal as described by Coleman *et al.*[12] It is therefore desirable to prevent the arrival of the prompt start pulses at the TAC input, and this is accomplished through the superimposition of suitably phased (i.e., undelayed) inverted stop pulses. The start rate is thereby further reduced to about 10 sec^{-1}, of which about 1 sec^{-1} correspond to slow positrons.

A principal aim of the present experiment was the achievement of good signal-to-background ratios in the time spectra of positrons having energies less than a few eV. Although the signal time spectrum dN/dt is peaked, whereas the background component decays exponentially with a time constant of 2 μsec (the reciprocal of the stop pulse rate), the signal energy distribution dN/dE is spread over an increasing number of time channels as the positron energy E decreases:

$$\frac{dN}{dt} \propto E^{1.5}\frac{dN}{dE} . \tag{1}$$

As a result, the signal time spectra recorded by Canter *et al.*[2] for positrons having mean energies less than a few eV were very widely spread over the background component. The time width W of a signal spectrum is proportional to the length of the flight tube. Therefore, in order to minimize W and thereby maximize the signal-to-background ratio, the tube length was made as short as possible.

III. DATA ANALYSIS

Figure 2(a) shows a typical MCA time spectrum with 3 V accelerating potential applied to the MgO coated grid. Because of the reversal of the timing roles of the emission and annihilation pulses described in Sec. II, real time increases from right to left on the spectrum; the vetoed prompt peak, which defines true time zero, occurs on the extreme right (marked VR). Prior to transforming the signal time distribution into an energy spectrum, the signal restoration and background substraction procedures described by Coleman *et al.*[13] are employed, using the simplified formulas for the case where the stop pulse rate swamps the signal pulse rate. The method requires that the total numbers of accepted start and input stop pul-

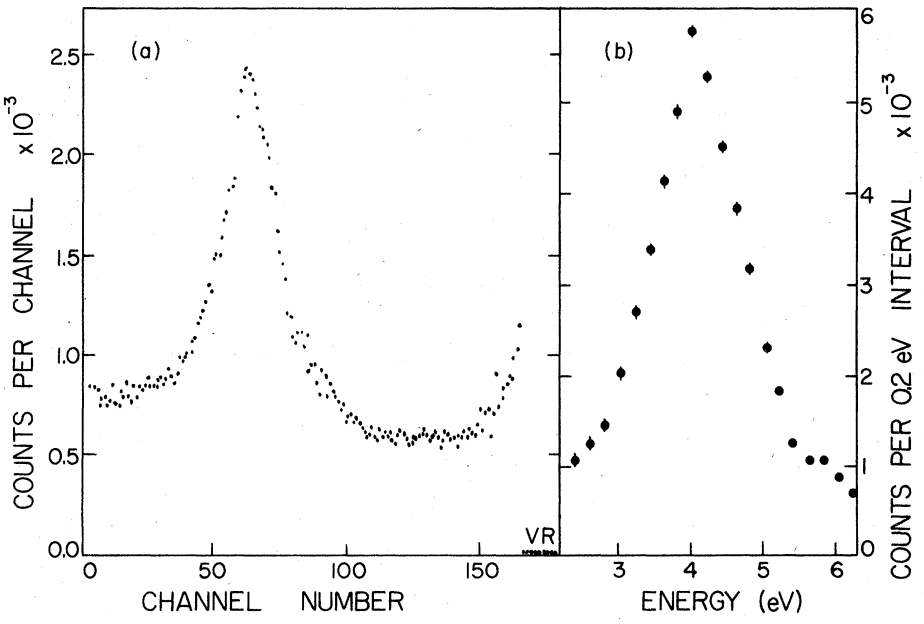

FIG. 2. (a) MCA time spectrum for $V = 3$ V; 4.22 nsec per channel. (b) Energy spectrum derived from (a). VR, veto region.

ses are recorded during each run. The appropriate start pulses, counted by a fast scaler, are those TAC "true start" pulses which are coincident with SCA output pulses. (See Sec. II.) The stop pulses to be counted are obtained from the emission discriminator and a correction is made for its 35-nsec dead time. The time calibration technique of Coleman *et al.*[13] is also employed.

The counts in the isolated, signal time spectrum are next redistributed into energy "bins" of equal width in the following manner. Time zero is first determined to within 0.1 channel width, for each TAC time range and stop pulse delay used, by removing the vetoing facility and measuring the centroid of the prompt signal peak thereby accumulated. A correction, measured to be 1.4 nsec, is applied to the centroid position to account for the transit time of fast positrons and gamma rays from source to target.

Equivalent positron energies are next assigned to the end of each time channel. Since the energies of interest are those possessed by the positrons between the grounded tungsten grids at each end of the flight tube, the total time t_d spent in the two accelerating fields is first estimated and subtracted from the total measured flight time t_f at the limit of each channel. Assuming a value for the flight path length d, energies E are then calculated from the remaining times $t \equiv t_f - t_d$:

$$E = 284.3 d^2/t^2, \tag{2}$$

where the units of E, d, and t, are eV, cm, and ns, respectively. A rapidly convergent iterative adjustment of E is then made as the small correction $t_d(E)$ becomes increasingly better determined. Finally, the energy spectrum is constructed by summing the counts in the channels and fraction of channels of the time spectrum which lie beneath the fixed limits of each energy bin (typically of widths 0.2 or 0.5 eV). The application of this procedure to the time spectrum of Fig. 2(a) results in the energy spectrum shown in Fig. 2(b).

It is clear that spectra constructed in this way are truly representative of positron energy distributions only if (a) there is little time jitter associated with the moderation-emission mechanism; (b) the angular spread of the beam is small; (c) the increase in path length d resulting from spiralling induced by the curved axial magnetic field is independent of positron energy; and (d) the timing resolution of the system does not appreciably widen the spectrum. Conditions (a) and (b) will be discussed in Sec. IV. Condition (c) has been explored by Kauppila *et al.*,[14] who point out that provided the curvature of the magnetic field is gradual, no additional spiralling is induced; thus positrons leaving the moderator axially would simply follow the field lines to the target. The close agreement of the length of the flight path measured by the TOF technique (see Sec. V) and the physical length of the flight tube supports this proposition. Condition (d) is violated for spectra centered at about 11 eV or higher and the implications are discussed in Sec. V.

IV. MODERATOR CHARACTERISTICS

An apparently correlated broadening of the positron energy spectrum and a shift towards a higher mean energy are observed, with the moderator undisturbed, in the first few days after the installation of a newly prepared MgO coated grid into the system. It is reasonable to postulate that the oxide powder grains, under constant positron bombardment, are left with a net positive charge whose size depends upon the physical state of the powder and which is largely responsible for the observed spread of positron energies. As the net electrostatic accelerating field produced by the oxide potential would be essentially normal to the plane of the oxide support grid, the spread in angles between the emitted positron velocities and the flight tube axis should be small. Near-normal emission was also reported by Costello *et al.*[1] Further support for this picture is supplied by the results of Killeen[15] who simulated a series of TOF spectra using the Monte Carlo technique, and by the behavior of scattering cross sections with energy across the measured energy spectra (see Sec. V).

In Fig. 3 the slow-positron yield, the FWHM of the energy spectra, and the difference between the mean positron energy $\bar{E}$ and the accelerating potential V are plotted versus V. For these measurements, as for the majority of the experimental runs, the axial magnetic field strength was reduced to a level at which only about 80% of the slow positrons reached the target in vacuum, varying typically from 4 G for $V = 0$ to about 12 G for $V = 30$ V (see Fig. 4).

The widths of the time spectra in Fig. 3 have been corrected for the time resolution τ_R of the system, measured to be 4.4 ± 0.1 ns. The correction is sizeable only for peaks where $\bar{E} > 10$ eV (e.g., 50% at $\bar{E} = 15$ eV). The variation of FWHM with V appears to be correlated with that of $(\bar{E} - V)$ discussed below, and is attributed to changes in the positron energy distributions rather than to other possible causes such as the effects of emission time jitter, angular spread in the emission direction of moderated positrons, or magnetic field inhomogeneities.

The decrease in $\bar{E} - V$ with increasing V between 0 and 10 V is tentatively attributed to a polarization of the charge distribution retained by the MgO layer, which reduces the effective accelerating

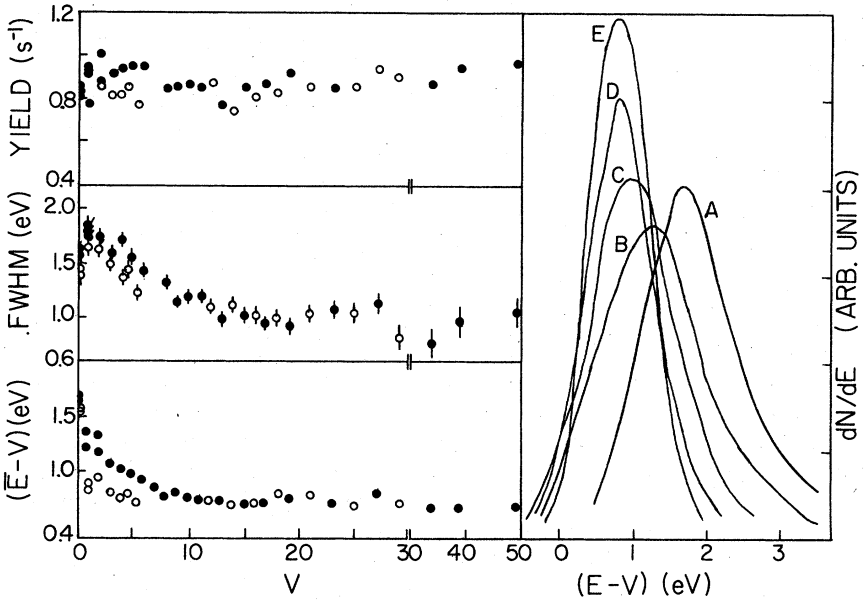

FIG. 3. Slow-positron energy spectrum parameters (defined in text) vs accelerating voltage V. Spectra A, B, C, D, and E are for $V=0$, 1, 3, 8, and 10 V, with first-order time-resolution corrections applied.

potential V_{eff} experienced by the emitted slow positrons. As V approaches 10 V, $V-V_{eff}$ approaches a limit of 0.8 eV, which is then maintained as V is then reduced to as low as 1 V (open circles in Fig. 3) and is destroyed only by grounding the grid. This effect is consistent with a model in which more energy is required to polarize the charged granules initially than to maintain subsequently the achieved state of polarization.

The effects of magnetic field inhomogeneities on the TOF signal spectra were monitored by varying the current through any or all of the four solenoids used. Small changes in the centroid position and large reductions in the measured yield were noted. The chosen course of action, i.e., the passage of current through the series-connected solenoids so as to allow 80% slow-positron transmission, was based partly on these observations and partly on the requirements of the experiment and appears to minimize the effects of field nonuniformities. That some slight path distortion might remain is suggested by the path-length determination results discussed in Sec. V A.

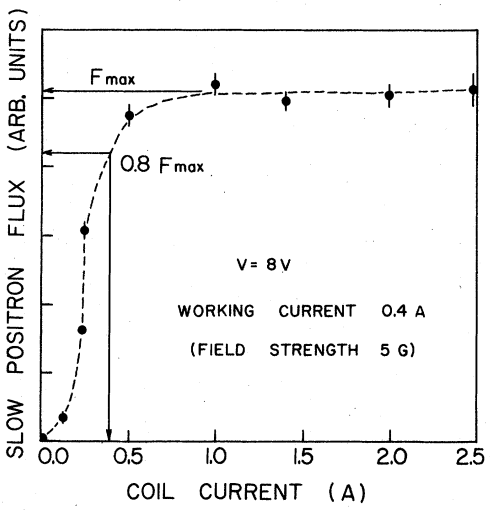

FIG. 4. Timed slow-positron flux vs coil current Flight tube evacuated. F_{max} represents the transmission of all the forward-going slow positrons emitted from the MgO to the target.

V. CROSS-SECTION DETERMINATION AND ERRORS

A. Path-length determination

A positron energy-independent path length of 0.329 m, which is 6 mm longer than the axial path length, was used in the calculation of the $\bar{E}-V$ values plotted in Fig. 3. When the shorter path length $d=0.323$ m is used, the calculated $\bar{E}-V$ values continue to decrease with increasing accelerating potential and would thus be consistent with nonsaturation of the charge polarization discussed in Sec. IV. However, in addition to the "well-behaved" relation between $\bar{E}-V$ and V which results for $d=0.329$ m, the choice of this value is also supported by the scattering cross sections measured for helium, which are inversely proportional to d. The present values are in good agreement at energies above 18 eV with two earlier sets of measurements by other investigators (see Sec. VI). In contrast, adoption of $d=0.323$ m results in a large systematic difference in this energy region; cross sections are increased by 2%

and energies are decreased by 4% (i.e., by 1 eV or more).

The path-length value of 0.329 m was, therefore, determined by requiring $\bar{E} - V$ to remain constant above $V = 10$ V. Deviations from this constancy were detectable when the path length was varied by 0.5 mm, equivalent to a precision of better than 0.2%.

B. Cross-section calculation procedures

The procedure for calculation of total cross sections is illustrated in Fig. 5. The total numbers of positrons in each 0.5-eV wide energy bin across energy spectra accumulated with and without gas in the flight tube—I and I_0, respectively—were measured. The total cross section Q for each bin is attributed to the mean energy of that bin and is calculated from

$$Q = \ln(I_0/I)/nd, \tag{3}$$

where n is the number density of gas atoms and $d = 0.329$ m is the path length. Because at low energies the accelerating potential was generally changed by 1 V or less, considerable energy overlap occurred between consecutive pairs of energy spectra. Therefore, the final Q values were taken as the weighted means of a number of measurements from different bins of different peaks. Cross sections calculated across any single pair of peaks agree within statistical deviations with the final mean cross sections, which are predominantly weighted by values derived from the central portions of the peaks. This result strongly supports the assumption of small angular divergence in the beam.

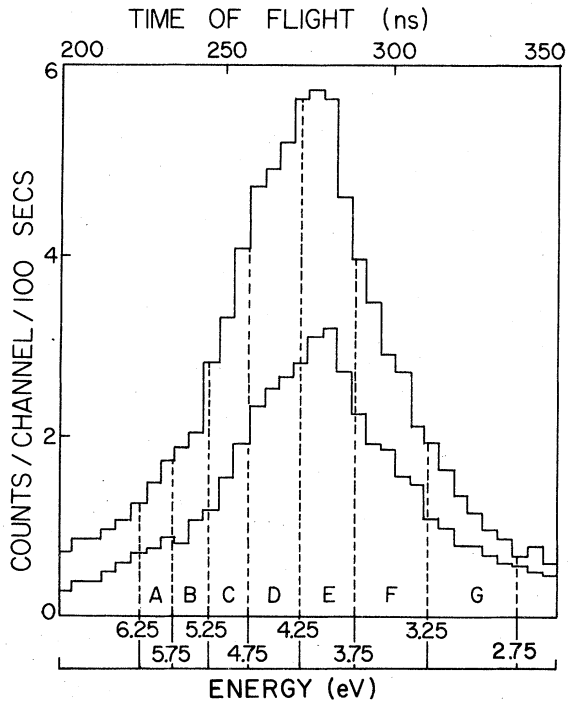

FIG. 5. Pair of MCA histograms, collected with the flight tube evacuated and filled with neon at 10 mTorr. The ratios of counts in bins A to G, between set energy limits, are used to calculate total cross sections which are attributed to the mean positron energy in each bin. The seven cross sections from the above spectra agree within statistical uncertainties with the mean cross sections plotted in Fig. 7.

At energies above 11 eV, the values of Q were obtained using only the central portions of the energy peaks and are atttributed to $\bar{E}$. This is done since time resolution smearing here renders the splitting of the spectra into the energy bins meaningless.

A waiting period of between 5 and 8 h was generally imposed before data collection commenced after changing the accelerating potential. For changes of as little as 1 V, some initial instability, i.e., peak drift of the order of 0.1 eV, was noted. Even drifts as small as these are sufficient to change significantly the values of Q calculated from positron counts taken from steeply sloping peak sides. They are interpreted as being a remnant of the much larger effects discussed in Sec. IV.

C. Experimental errors

Gas pressures ranging from 0.005 to 0.1 Torr, for which the Baratron reading uncertainties are quoted by the manufacturer as less than 0.1%, were used during the course of the experiment. Steady pressure drifts of about 1% in 12 h, attributed to gas input valve instability, were sometimes observed, in all cases the mean of the pressure readings taken before and after a run were used in the calculations. The effect of thermal transpiration on Baratron readings has been discussed by Kauppila *et al.*,[14] who apply a correction to their measured pressure P_m according to

$$P = P_m(T/T_m)^{1/2}, \tag{4}$$

where T and T_m are the temperatures of the flight tube and gauge head ($T_m \simeq 322$ K). The correction is thus about 4% for $T = 297$ K. However, use of the full equation of Liang,[16] which enables calculation of P/P_m as a function of gas number density and the diameter of the tube connecting the gauge head to the system, yields corrections for the present apparatus of less than 0.25% for helium and 0.5% for neon. These corrections have been applied to the results presented in Figs. 6 and 7 and are in reasonable agreement with the experimentally determined corrections of Bromberg,[17] who measured a maximum transpiration effect of

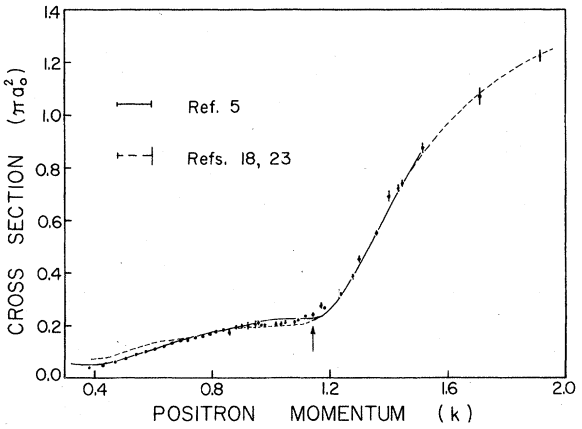

FIG. 6. Total scattering cross sections for positron-helium collisions. Error bars lie within size of points unless shown. Solid and broken lines are smoothed fits to the data points of Refs. 5 and 23, respectively, with typical error bars at the limits of the lines shown in the top left corner. The inelastic threshold energy (for Ps formation) is indicated by the arrow.

1.1% which was pressure independent below $P \simeq 10$ mTorr.

The size of the total uncertainty in pressure readings is estimated to be less than 0.5% and, since most of the reported cross sections are means of several separate measurements, the total contribution to the uncertainty in Q from inaccuracies in pressure measurement is estimated to be a fraction of 1%.

The determination of path length was described in Sec. V A, and a precision of better than 0.2% was quoted. Changes in the Q values arising from the use of the axial path length would be within statistical deviations below 10 eV and become important only at higher energies. The adoption of $d = 0.329$ m may thus be considered as "fine tuning," i.e., the use of the sensitivity of Q and $\bar{E}$ to d at the higher energies to determine more precisely cross sections at lower energies.

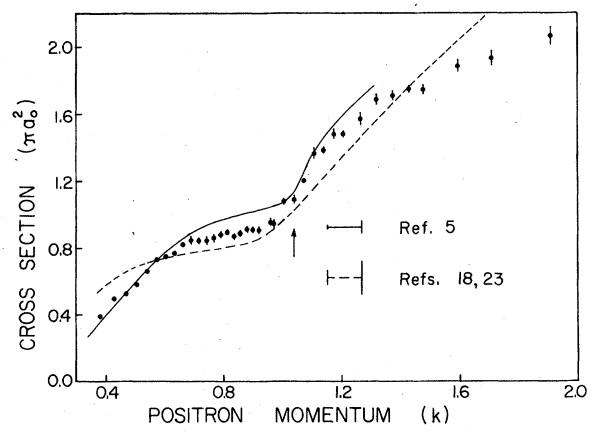

FIG. 7. Total scattering cross sections for positron-neon collisions. The presentation of data follows the conventions of Fig. 6.

In many of the early runs using high magnetic fields and in later runs at the highest and lowest positron energies, a systematic decrease was observed in the cross sections calculated on the low-energy (long-time) side of the signal spectra. This is symptomatic of the detection of forward-scattered positrons, a problem common to all positron beam transmission systems. Positrons scattered through small forward angles are constrained by the magnetic field and are annihilated at the target after a time interval longer than the TOF of unscattered positrons of the same energy. Some scattered positrons may possess flight times lying within the unscattered positron TOF spectra so that an energy peak measured with gas in the system can be distorted to a degree greater than that expected from the variation of Q between the limits of the peak.

Using a high axial magnetic field strength of 30 G, attenuated (gas) peaks with mean energies of a few eV were found to possess more counts in the long-time tail than did their associated vacuum peaks, thus yielding negative cross sections and confirming the detection of scattered positrons. If a fraction f of the scattered positrons is collected with the unscattered peak, the resulting percentage error in Q for an observed attenuation of 2:1 is $\sim 140f$ for f up to 0.4.

The detection of scattered positrons is minimized by reducing the magnetic field strength to the lowest practical level, as discussed in Sec. IV. The success of this procedure was judged by comparing cross sections calculated from energy divisions at the same mean energy occurring at different positions on different pairs of spectra. The number of scattered positrons detected on the short-time side of a peak would be very small, and the true cross-section values would here be closely approached. Under routine operating conditions, agreement within statistical uncertainties was found between cross-section values deduced from the short-time and long-time sides of peak pairs and no systematic trends were evident for energies less than 25 eV. For larger energies, the cross-section value on the short-time side of the peak was taken, following the procedure of Coleman *et al.*[18]

There presently exists no method for verifying the cross sections calculated from the low-energy sides of the peaks with the lowest mean energies. Energy bins centered at 2 eV still occur on both the high- and low-energy sides of different peaks and, for this reason, only values at and above 2 eV are reported. However, at 1.0 and 1.5 eV the

cross sections measured for Ne are in reasonable agreement with those reported by Stein *et al.*,[5] whereas for helium they lie about 30% below their values. (See Sec. VI.)

In the determination of the path length, it was assumed that the amount of scattering occurring within the two regions where the positrons are accelerated is negligible. Once within 5 mm of the target, positrons are drawn to their annihilation by a 3×10^4 V m^{-1} electrostatic field whether they are scattered or not. Scattering in this region is, therefore, not detectable and 5 mm is accordingly excluded from the flight path. Scattering in the 2-mm gap between the MgO coated grid and the grounded grid, in which the positrons are accelerated after moderation, does contribute to the measured attenuation of the gas spectra. Corrections for this effect of 0.3% to 0.1% between 2 and 50 eV have been applied to the He data, and of 0.3% to 0.15% over the same energy range have been applied to the Ne data.

VI. CROSS-SECTION RESULTS

The present experimental results for the total cross sections for positrons scattered from He and Ne atoms as a function of positron momentum are presented in Figs. 6 and 7, respectively. The cross-section measurements for He were briefly reported by Burciaga *et al.*[19] Other recently measured values are shown for comparison.

In Fig. 8(a) the measured cross sections are compared with several recent theoretical results for elastic scattering in He. The most elaborate of these, the variational calculation of Campeanu and Humberston,[20] diverges from the measured data points only below $k=0.7$ (7 eV), in which region there is close agreement between the present measurements and those of Stein *et al.*[5]

Figure 8(b) compares the Ne results with the recent elastic scattering calculations of McEachran *et al.*[21] and with those of Montgomery and Labahn.[22] Both are polarized orbital calculations, and inclusion of virtual positronium formation is expected to increase the Q values somewhat at the high-energy end of the elastic scattering region.

In summary, agreement among the present cross cross-section results and earlier experimental and theoretical values is marginally satisfactory for He, with the major discrepancies occurring below 7 eV. The agreement is less satisfactory for Ne.

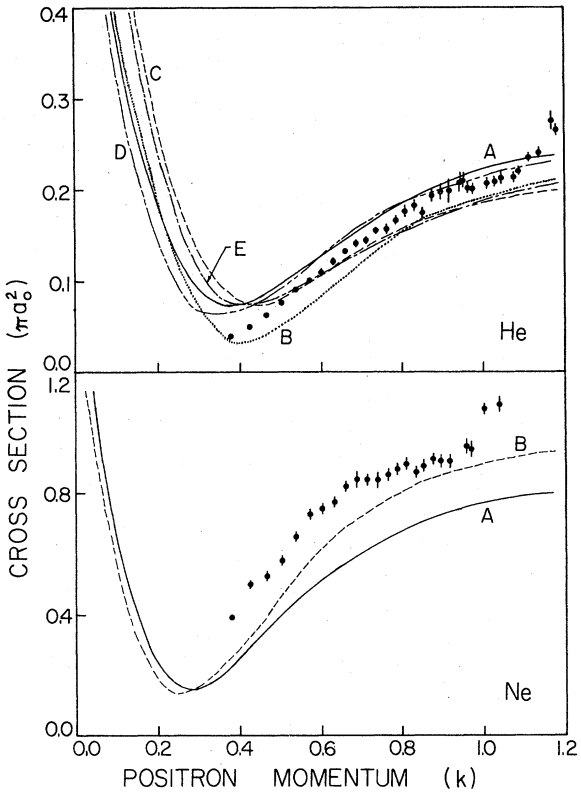

FIG. 8. Comparison of total cross sections for He and Ne (below inelastic thresholds) with theoretical calculations. Helium (top), curves A, B, C, D, and E are from Refs. 20 and 24–27, respectively. Neon, curves A and B are from Refs. 22 (2*S*–*P* and 2*P*–*D* norm) and 21, respectively.

The major implication of the results of the study of the behavior of the MgO moderator is that the characteristics of the spectrum of energies of the emitted positrons is largely dependent on the degree of charging of the powder granules. In order to measure reliably cross sections below 2 eV, further redesign of the spectrometer system is planned. Methods for arresting the charging of the oxide are being tested.

ACKNOWLEDGMENTS

This research was supported in part by the Robert A. Welch Foundation, Houston, Texas 77002 and by the National Science Foundation under Grant Nos. SMI76-83578 and SPI76-83578 A01. The authors would like to thank J. T. Hutton and J. A. Platt for technical assistance.

*Present address: Dept. Physics, Texas A & M University, College Station, Tex. 77843.

[1]D. G. Costello, D. E. Groce, D. F. Herring, and J. Wm. McGowan, Can. J. Phys. 50, 23 (1972).
[2]K. F. Canter, P. G. Coleman, T. C. Griffith, and G. R. Heyland, J. Phys. B 5, L 167 (1972).
[3]B. Jaduszliwer and D. A. L. Paul, Can. J. Phys. 51, 1565 (1973).
[4]W. E. Kauppila, T. S. Stein, and G. Jesion, Phys. Rev. Lett. 36, 580 (1976).
[5]T. S. Stein, W. E. Kauppila, V. Pol, J. H. Smart, and G. Jesion, Phys. Rev. A 17, 1600 (1978).
[6]K. F. Canter, A. P. Mills, Jr., and S. Berko, Phys. Rev. Lett. 34, 177 (1975).
[7]D. W. Gidley, P. W. Zitzewitz, K. A. Marko, and A. Rich, Phys. Rev. Lett. 37, 729 (1976).
[8]S. Pendyala, D. Bartell, R. E. Girouard, and J. Wm. McGowan, Phys. Rev. Lett. 33, 1031 (1974).
[9]R. M. Nieminen and C. H. Hodges, Solid State Commun. 18, 1115 (1976).
[10]S. Pendyala, D. Bartell, F. E. Girouard, and J. Wm. McGowan, Can. J. Phys. 54, 1527 (1976).
[11]T. S. Stein, W. E. Kauppila, and L. O. Roellig, Phys. Lett. A 51, 327 (1975).
[12]P. G. Coleman, T. C. Griffith, and G. R. Heyland, J. Phys. E 5, 377 (1972).
[13]P. G. Coleman, T. C. Griffith, and G. R. Heyland, Appl. Phys. 5, 223 (1974).
[14]W. E. Kauppila, T. S. Stein, G. Jesion, M. S. Dababneh, and V. Pol, Rev. Sci. Instrum. 48, 822 (1977).
[15]T. L. Killeen, Ph.D. thesis (University of London, 1975).
[16]S. C. Liang, Can. J. Chem. 33, 279 (1955).
[17]J. P. Bromberg, J. Vac. Sci. Technol. 6, 801 (1969).
[18]P. G. Coleman, T. C. Griffith, G. R. Heyland, and T. R. Twomey, Appl. Phys. 11, 321 (1976).
[19]J. R. Burciaga, P. G. Coleman, L. M. Diana, and J. D. McNutt, J. Phys. B 10, L569 (1977).
[20]R. I. Campeanu and J. W. Humberston, J. Phys. B 8, L244 (1975).
[21]R. P. McEachran, A. G. Ryman, and A. D. Stauffer J. Phys. B 11, 551 (1978).
[22]R. E. Montgomery and R. W. Labahn, Can. J. Phys. 48, 1288 (1970).
[23]K. F. Canter, P. G. Coleman, T. C. Griffith, and G. R. Heyland, Appl. Phys. 3, 249 (1974).
[24]H. Aulenkamp, P. Heiss, and E. Wichmann, Z. Phys. 268, 213 (1974).
[25]R. P. McEachran, D. L. Morgan, A. G. Ryman, and A. D. Stauffer, J. Phys. B 11, 951 (1978).
[26]M. Ya Amusia, N. A. Cherepkov, L. V. Chernysheva, and S. G. Shapiro, J. Phys. B 9, L531 (1976).
[27]Y. K. Ho and P. A. Fraser, J. Phys. B 9, 3213 (1976). The *s*-wave phase shifts in this reference were combined with the higher-order phase shifts of Ref. 20.